AGU PUBLICATIONS

JGR

Journal of Geophysical Research: Atmospheres

RESEARCH ARTICLE
10.1002/2017JD027072

Key Points:
- TC inner-core lightning activity is less sensitive to SST increases but more sensitive to vertical wind shear compared to the outer rainband
- Rapidly intensifying TCs have the lowest flash density in the inner core but the highest flash density in the outer rainband
- Inner core flash density decreases 12–18 h preceding the onset of TC rapid intensification but increases 6–12 h before TC weakening

Correspondence to:
W. Xu,
wxinxu@atmos.colostate.edu

Citation:
Xu, W., S. A. Rutledge, and W. Zhang (2017), Relationships between total lightning, deep convection, and tropical cyclone intensity change, *J. Geophys. Res. Atmos.*, *122*, 7047–7063, doi:10.1002/2017JD027072.

Received 3 MAY 2017
Accepted 13 JUN 2017
Accepted article online 17 JUN 2017
Published online 6 JUL 2017

Relationships between total lightning, deep convection, and tropical cyclone intensity change

Weixin Xu[1], Steven A. Rutledge[1], and Wenjuan Zhang[2]

[1]Department of Atmospheric Sciences, Colorado State University, Fort Collins, Colorado, USA, [2]State Key Laboratory of Severe Weather, Chinese Academy of Meteorological Sciences, Beijing, China

Abstract This study investigates the characteristics of total lightning in the inner core (INCO, 0–100 km) and outer rainband (OB, 200–400 km) of tropical cyclones (TC). Relationships between flash density (FLD), convective intensity, and TC intensity change are further examined. FLD shows a bimodal structure with a strong maximum in the eyewall (INCO, 0–50 km) and a secondary maximum in the OB. FLD maximizes under conditions of warmest sea surface temperature (SST) and large values of vertical wind shear. Compared to OB FLD, INCO FLD is less sensitive to SST increase but shows greater variability in relation to shear. Intensifying TCs have substantially lower INCO (but higher OB) FLD compared to weakening and neutral TCs. Similar trends are shown in radar quantities (volume of 30 dBZ echoes in the mixed phase). rapidly intensifying (RI) TCs also show significantly smaller FLD and VOL30 than slowly intensifying TCs, indicating the potential of these parameters in forecasting RI. INCO (OB) FLD decreases (increases) 12–18 h preceding the onset of RI, while INCO (OB) FLD increases (decreases) 6–12 h prior to TC weakening. These relationships between lightning and TC intensity change (+24 h) are generally maintained regardless of prior (−24 h) TC intensity change status. However, convective depth and vertically integrated ice content in the INCO increased preceding TC intensification, suggesting the lack of supercooled liquid content and establishment of glaciated conditions (evident by an increase in the 20 dBZ and decrease in the 30 dBZ echo volume) in the INCO of intensifying TCs, especially RI.

1. Introduction

Despite dramatic improvements in forecasting tropical cyclone (TC) track in the last decade, forecasting TC intensity change remains a challenge [*DeMaria et al.*, 2014]. This is because TC intensity is not only affected by external factors such as sea surface temperature (SST), vertical shear, and lower tropospheric humidity [*Kaplan and DeMaria*, 2003] but is also modulated by episodic convective-scale processes within the inner core (INCO) region [*Hendricks et al.*, 2010]. In recent years, the role of INCO deep convection has been widely considered to be an important factor in TC intensification, marked by an increase in TC maximum sustained winds (MSW). Satellite imagery and airborne Doppler observations indicate that intensifying TCs have more frequent outbursts of intense convection in the eyewall compared to neutral TCs [*Steranka et al.*, 1986; *Rogers et al.*, 2013]. The possibility of TC intensification (within ±6 h) increases remarkably (from 17% to 82%) when one or more "hot towers" exist in the eyewall [*Kelley et al.*, 2004, 2005]. Rapidly intensifying TCs also have a greater number of overshooting tops than slowly intensifying and steady state TCs as revealed by satellite infrared imageries [*Griffin*, 2017]. Other satellite-based studies indicate that TC intensification is strongly correlated with increasing radar echo top heights and stronger depression of microwave brightness temperatures owing to ice scattering [*Jiang*, 2012; *Jiang and Ramirez*, 2013]. Model simulations also emphasized the importance of hot towers and convective bursts near the eye during TC rapid intensification [*Rogers*, 2010; *Guimond et al.*, 2010]. A TC warm core can rapidly develop if deep convection occurs within the radius of MSW in the INCO region [*Vigh and Schubert*, 2009]. Asymmetric deep convection, e.g., intense "vortical hot towers," can generate potential vorticity anomalies or transform a midlevel vortex into a near-surface vortex, with both leading to vortex intensification [*Hendricks et al.*, 2004; *Montgomery et al.*, 2006]. *Montgomery and Smith* [2011] further emphasized the importance of asymmetric heating due to submesoscale deep convection in the spin-up of TC INCO winds. However, recent studies showed that symmetric distribution of convection in the INCO, especially shallow-to-moderate convection, is the most marked feature distinguishing rapidly intensifying (RI) and non-RI TCs [*Tao and Jiang*, 2015; *Alvey et al.*, 2015]. These observational findings supported previous numerical studies emphasizing symmetric heating in TC intensification [*Nolan and Grasso*, 2003; *Nolan et al.*, 2007], which found that asymmetric heating has a very small impact on vortex

intensification. *Tao and Jiang* [2015] argued that RI is triggered by increases in symmetric shallow-to-moderate convection, whereas asymmetric deep convection is more likely a response to vortex intensification during RI.

As an indicator of intense convection, lightning was also found to be closely associated with TC intensity change [*Molinari et al.*, 1999]. Many studies reported eyewall lightning outbreaks slightly prior to or during TC intensification [*Lyons and Keen*, 1994; *Squires and Businger*, 2008; *Stevenson et al.*, 2014; *Zhang et al.*, 2015]. For example, lightning bursts inside the radius of MSW were found to precede rapid intensification by 6 h in Hurricane Earl (2010) (Atlantic basin) [*Stevenson et al.*, 2014; *Susca-Lopata et al.*, 2015]. Remarkable eyewall lightning outbreaks during periods of RI, eyewall replacement cycle, and maximum intensity were observed in Rita (2005) and Katrina (2005), two of the strongest storms in the Atlantic hurricane record [*Squires and Businger*, 2008]. Based on 5 years of TC samples in the northwestern Pacific basin, *Zhang et al.* [2015] showed that RI TCs exhibit substantially higher INCO lightning density than rapidly weakening (RW) TCs, although INCO lightning density in RI and neutral TCs was similar. Other studies found a strong positive correlation ($r = 0.7–0.8$) between lightning frequency and MSW in major hurricanes when the entire TC region is included [*Price et al.*, 2009; *Pan et al.*, 2014; *Whittaker et al.*, 2015]. These latter studies showed that TC peak intensity is preceded (~24 h) by increased cloud-to-ground (CG) lightning activity. *Whittaker et al.* [2015] further demonstrated that time scales of lightning leading TC winds are highly dependent upon the TC area used for the lightning estimation. Lightning density in the outer rainband (OB) region is more likely to increase prior to TC intensification [*DeMaria et al.*, 2012; *Stevenson et al.*, 2016].

However, a statistical negative relationship between INCO lightning and TC intensity change (i.e., significant increase of INCO lightning in weakening TCs compared to intensifying TCs) was reported for North Atlantic and eastern North Pacific TCs [*DeMaria et al.*, 2012; *Stevenson et al.*, 2016], leading to the conclusion that lightning bursts in the INCO may be indicative of the end of TC intensification. Similarly, *Thomas et al.* [2010] found an increase in the relative number of positive CG lightning flashes in the INCO of three weakening Atlantic TCs. *DeMaria et al.* [2012] hypothesized that the observed relationship between INCO lightning activity and TC intensity change could be explained by the interaction of environmental shear with high potential vorticity (PV) in the INCO [*Davis et al.*, 2008] and/or the eyewall replacement process [*Kossin and Sitkowski*, 2009]. Environmental shear can tilt the vertical column of very high PV in the TC INCO region and cause secondary upward motion due to vortex balance [*Davis et al.*, 2008; *Corbosiero and Molinari*, 2003]. Strongly sheared environments may disrupt the TC's INCO structure and reduce the organization of eyewall convection leading to convective dissipation. *Molinari et al.* [1999] suggested that the sign of the intensity change may be dependent on prior intensity changes, where weakening or slowly intensifying TCs are likely to intensify after a lightning outbreak in the INCO.

To date most TC lightning studies used ground-based measurements from the National Lightning Detection Network (NLDN) [*Black and Hallett*, 1999; *Molinari et al.*, 1999] and the World Wide Lightning Location Network (WWLLN) [*Price et al.*, 2009; *DeMaria et al.*, 2012; *Pan et al.*, 2014; *Zhang et al.*, 2015; *Whittaker et al.*, 2015; *Stevenson et al.*, 2016]. While the NLDN detects lightning only within a few hundred kilometers of land, the WWLLN detects mainly CG lightning over open oceans (and land). There are benefits of using total lightning data (including intracloud and CG) compared to CG-only data. Intracloud (IC) lightning has been shown to be an excellent surrogate for convective vigor and strong updrafts [*Lang and Rutledge*, 2002], while CG information has been found to be mostly indicative of reflectivity core descent, which may at times indicate collapse of an updraft [*Reap and MacGorman*, 1989; *Lang et al.*, 2000]. The IC:CG ratio has been shown to vary greatly from 3:1 in average thunderstorms to as much as 100:1 in some severe continental storms [*Boccippio et al.*, 2001; *McCaul et al.*, 2002]. Therefore, total lightning may provide more detailed information on storm structure and microphysics compared to CG alone. Comparatively fewer observational [*Fierro et al.*, 2011] and modeling studies [*Fierro and Reisner*, 2011; *Fierro et al.*, 2015] have shown the importance of total lightning for TC intensification and forecasting. With the recent launch of GOES-R Geostationary Lightning Mapper [*Goodman et al.*, 2013], soon providing continuous total lightning observations over most of the TC regions of the Atlantic and eastern North Pacific TC basins, the application of total lightning observations in forecasting TC intensity change is now a very achievable objective.

Based on 2 years of total lightning observations from the Optical Transient Detector (OTD), *Cecil and Zipser* [1999] found no clear relationship between total lightning activity and TC intensification. *Jiang and*

Ramirez [2013] reported a generally negative relationship between INCO total lightning and TC intensity change based on precipitation features derived from the Tropical Rainfall Measuring Mission (TRMM) satellite. To go beyond the aforementioned studies, we analyzed 16 years of total lightning observations from the Lightning Imaging Sensor (LIS) on board TRMM. The LIS detects total lightning flashes with a flash detection efficiency of 70–90% [*Christian et al.*, 2003]. While ground-based networks (e.g., WLLNN) monitor lightning activity continuously, the LIS observes lightning in a 1–2 min period during a satellite overpass and is thus unable to provide temporal evolution of individual storms. However, it is reasonable to assume that the long record of TC overpasses by TRMM well samples the full spectrum of the TC life cycle. In this study we will also examine observations from the precipitation radar (PR), the microwave imager (TMI), and the visible/infrared imager (VIRS) regarding convective intensity and mixed-phase precipitation microphysics.

This study first examines the characteristics of TC total lightning in all TC basins (section 3), in terms of lightning occurrence frequency, flash rate, flash density, radial distribution, and flash density as a function of SST and shear. We further address several fundamental questions regarding the relationship between total lightning, intense convection, and TC intensity change (section 4): (1) Does total lightning show similar relationships to TC intensity change compared to CG lightning [e.g., *DeMaria et al.*, 2012]? (2) Does the total lightning-TC intensity change relationship vary between INCO and OB, and if so, what factors contribute to this behavior? (3) Is increasing or decreasing total lightning a leading signal for RI, if so, what are characteristic lead times? (4) Do TRMM radar observations of intense convection show similar relationships to TC intensity change as does lightning flash density (LIS)? (5) Does the relationship between lightning and TC intensity change depend on prior (e.g., −24 h) intensity change status (e.g., neutral or has been weakening)?

2. Data and Methodology

2.1. Selection of TRMM Individual TC Overpasses (ITPs)

This study examines TCs in all six TC-prone basins including the Atlantic, Eastern Pacific, Northwest Pacific, Southwest Pacific, Northern Indian Ocean, and Southern Indian Ocean. We use the 6-hourly TC best track data from the International Best Track Archive for Climate Stewardship (IBTrACS) [*Knapp et al.*, 2010] and version 7 TRMM level 1 orbital data [*Kummerow et al.*, 1998] during the period 1998–2013. We selected all TRMM overpasses of TCs reaching at least tropical storm category (MSW $\geq$ 34 kt) during the TC life cycle. For the TC intensity, tropical depression (TD) are defined as MSW between 0 and 33 kt, tropical storm (TS) as MSW between 34 and 63 kt, category 1 to 2 (CAT12) as MSW between 64 and 95 kt, and category 3 to 5 (CAT35) as MSW $>$ 95 kt. TC center location and intensity (MSW) during the TRMM overpass time were linearly interpolated from the 6-hourly data using IBTrACS. TRMM overpasses associated with any missing intensity values in the 6-hourly IBTrACS were excluded.

To minimize land effects on TC convective structure and intensity change, the sample is restricted to ITPs with TC centers $>$ 100 km from the nearest coastline (defined by storm distance from land in IBTrACS). The sample also excludes TC stages during and after extratropical transitions (defined in IBTrACS). In order to ensure a significant fraction ($>$40%) of the TC INCO region (e.g., 0–100 km) is sampled by LIS, which has a 680 km wide field of view after the TRMM boost in 2001 (Figure 1a), the sample is constrained in such a way that the distance between the TC center and the TRMM central line is no greater than 350 km (Figures 1a and 1b). In our TC data set, the mean TC areal coverage (within 500 km radius) by LIS (with view time $>$ 1 min) is 57%. After considering the aforementioned constraints, a final set of 8587 TC periods from 1401 TCs sampled by TRMM were selected for analysis (Table 1), which we define as individual TC overpasses (ITPs). Geographical distributions of these ITPs (in different TC intensity categories) are shown in Figure 1c.

2.2. TC Total Lightning and TRMM Convective Parameters

Similar to previous studies [*Kelley et al.*, 2004; *DeMaria et al.*, 2012; *Tao and Jiang*, 2015], the TC area (or an ITP) is defined within 500 km in radius from the TC center as shown in Figure 1. Considering the variability of the eyewall extent [*Jiang et al.*, 2013], limited sample in the eyewall (tens of kilometers in width), and consistency with previous studies [*DeMaria et al.*, 2012; *Zhang et al.*, 2015; *Stevenson et al.*, 2016], INCO, and OB are defined as areas within 0–100 km and 200–400 km radius of the TC center, respectively. Compared to the data set with INCO identified manually [*Jiang and Ramirez*, 2013], the fixed (0–100 km) INCO definition yields only trivial differences concerning the statistics of INCO deep convection [*Tao and Jiang*, 2015].

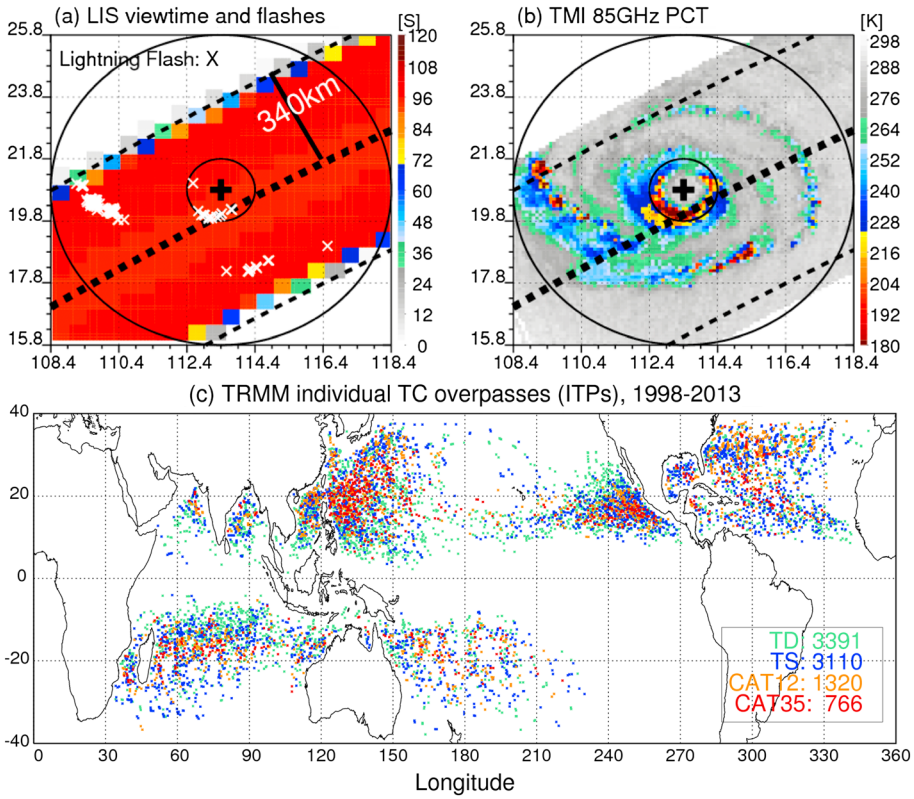

Figure 1. An individual TC overpass (ITP) example and locations of all selected ITPs during 1998–2013. (a) LIS view time (color shaded) and LIS-observed lightning flashes and (b) TMI microwave polarization-corrected brightness temperature at 85 GHz, both for the TRMM overpass of Typhoon Hagupit (2008) at 0721 UTC on 12 July 2002. (c) Locations of all ITPs > 100 km from the coast of different TC intensity categories. In Figures 1a and 1b, the TC center is marked by the bold plus sign, and the two solid circles denote 100 and 500 km from the TC center, respectively. TRMM central line is represented by bold dashed line, and the edge of LIS field of view is marked by thin dashed line.

Selected TRMM variables from LIS, PR, TMI, and VIRS are interpolated onto Cartesian grids of 10 km horizontal resolution (and 250 m vertical resolution for PR vertical profiles) within the ITP using the closest-point method (Figure 1). Since lightning is the primary interest of this study, TRMM data (e.g., TMI) outside the LIS viewing areas (680 km wide swath) are not considered (Figure 1b). Lightning flash rate (fl min^{-1}) is defined as total flash counts divided by the LIS view time ranging from 20 to 120 s (Figure 1a). Flash density (FLD), which has a unit of fl $(100\ km)^{-2}\ h^{-1}$, is further defined as flash rate divided by rain area estimated by TMI in the LIS field of view (Figure 1b). Here rain area (TMI rainrate > 0.1 mm h^{-1}) instead of total area [*DeMaria et al.*, 2012] is used for FLD calculation, given the noticeable difference in TC size (or rain area) across intensities and basins [*Knaff et al.*, 2007; *DeMaria et al.*, 2012]. *Jiang et al.* [2013] used a similar method to normalize lightning flashes, except that we further consider the variability of LIS view time (ranging 20–120 s) and swath difference between TMI (878 km, Figure 1b) and LIS (680 km, Figure 1a).

Table 1. TRMM Sampled TC Population and Individual TC Overpasses (ITPs), ITPs With Lightning, Mean Flash Rate, Mean Flash Density (FLD), and Mean Rain Area as a Function of TC Intensity (Category Definition in Section 2)[a]

	ALL	TD	TS	CAT12	CAT35
TCs	1401	1176	1038	489	283
All ITPs	8587	3391	3110	1320	766
ITPs w. lightning (frequency)	2955 (34%)	1097 (32%)	1067 (34%)	452 (34%)	339 (44%)
Mean Flash Rate (fl min^{-1})	3.6	3.1	3.9	3.6	3.9
Mean FLD (fl $(100\ km)^{-2}\ h^{-1}$)	15	15	16	14	13
Mean Rain Area ($10^5\ km^2$)	1.9	1.7	1.9	2.2	2.4

[a]Note that rain area is defined by areas (within the LIS field of view) having rain rate > 0.1 mm h^{-1} derived from TMI. The mean TC areal coverage (within 500 km radius) by LIS (with view time > 1 min) is 57%.

In parallel to FLD, a PR radar proxy (volume of 30 dBZ radar reflectivity in the mixed-phased region, VOL30) for convective intensity and mixed-phase microphysics is investigated. VOL30 has been suggested to be a good proxy of updraft intensity and lightning production [*Petersen et al.*, 1999; *Xu et al.*, 2010; *Liu et al.*, 2012]. In this study, VOL30 is defined as the total volume of radar pixels (≥30 dBZ) between 6 km (near −5°C) and 12 km (−40°C) deriving from PR reflectivity vertical profiles. VOL30 is further normalized by the precipitation area derived from PR to cancel PR sampling bias, e.g., lower (greater) VOL30 could be due to smaller (larger) PR coverage. This normalization is done through multiplying the VOL30 by the ratio of precipitation area of individual ITPs to the mean rain area of all ITPs (with INCO and OB areas separated).

In addition, we also examine TRMM proxies of convective depth (20 dBZ echo top height from PR, MAXHT20), vertically integrated ice content or ice scattering signature as defined by microwave polarization-corrected brightness temperature at 85 GHz (PCT85) [*Cecil and Zipser*, 1999; *Cecil et al*., 2002] from TMI, and cloud top temperature (infrared brightness temperature, IR Tb) from VIRS. To emphasize the role of deep convection, we only examine the highest (or coldest) 5% MAXHT20 echo top heights (PCT85 and IR brightness temperatures) in the INCO and OB. *Cecil et al.* [2002] suggested that only 2–4% of the TC precipitation corresponds to deep convective towers. Therefore, the top 5% echo top heights and Tb depression are argued to be reasonable proxies of deep convection from both the scale and intensity perspective.

2.3. Environmental Variables

To better understand the lightning-TC intensity change relationship, this study also investigates the environmental conditions (SST and vertical wind shear) underlying TC intensity change, and how lightning density varies as a function of SST and shear. SSTs are calculated using the daily SST data from the TRMM Microwave Imager and Advanced Microwave Scanning Radiometer for EOS [*Gentemann et al.*, 2010]. Environmental shear is derived from the European Centre for Medium-Range Weather Forecasts reanalysis Interim reanalysis data [*Dee and Uppala*, 2009], respectively. Mean SST of each ITP is the average SST within 500 km of the TC center [*Stevenson et al.*, 2016]. Environmental vertical wind shear is defined as the wind shear between 200 and 850 hPa ($V_{200} - V_{850}$) and averaged over a 500–750 km annulus around the TC center of each ITP, to remove the influence of the TC circulation [*Hence and Houze*, 2011].

3. Characteristics of TC Total Lightning

3.1. Occurrence Frequency, Flash Rate, and FLD

This study examined the total lightning characteristics of 8587 TRMM overpasses (ITPs) for 1401 individual TCs, including 766 major hurricane ITPs (Table 1 and Figure 1c). Approximately 35% of the total ITPs had at least one lightning flash (within 500 km of the TC center), resulting in an averaged flash rate of 3.6 flashes per minute and a FLD of 15 flashes per 10,000 km^2/h (Table 1). Based on the mean TC areal coverage by LIS (57%) and the lightning occurrence frequency of LIS-sampled ITPs (34%), the probability to have lightning somewhere within a 500 km radius from the TC center is estimated to be ~55%. The mean TC flash rate (3.6 fl min^{-1}) is roughly a factor of 5 smaller than continental thunderstorms, which is on the order of 10–20 fl min^{-1} [*Toracinta et al.*, 2002; *Cecil et al.*, 2015], suggesting the maritime nature of TC convection [*Cecil et al.*, 2002]. The TD category has the lowest lightning occurrence frequency (32%), whereas CAT35 storms have the highest (44%), possibly due to their greater storm size or precipitation area (Table 1). TS, CAT12, and CAT35 storms share similar flash rate magnitudes, although their TC size is different, while TD shows the lowest flash rate owing to its smallest storm size. However, TD/TS systems produce greater FLD than hurricanes/typhoons, consistent with previous studies using ground-based lightning measurements (mainly CG) [*Abarca and Corbosiero*, 2011; *Zhang et al.*, 2015; *DeMaria et al.*, 2012]. Compared to TD/TS, hurricanes/typhoons exhibit evident eyewall and rainband structure including well-defined inner rainband and interrainband regions where lightning is relatively rare [*Cecil et al.*, 2002; *Jiang et al.*, 2013]. Of the six TC basins, Atlantic and northwest Pacific events have the largest population of lightning-ITPs (Figure 2a). Significant TC lightning flash rates (>5 fl min^{-1}) generally occur over warmer oceans (>28°C) such as the Gulf Stream and eastern Pacific basin offshore from Mexico (Figure 2b). ITPs containing substantial lightning flashes (e.g., >30 fl min^{-1}) are mainly situated close to land (within 1000 km) possibly due to increase of coastal convergence, greater atmospheric instability [*Houze*, 2010], or increasing continental aerosol loading [*Khain et al.*, 2008] near the coast.

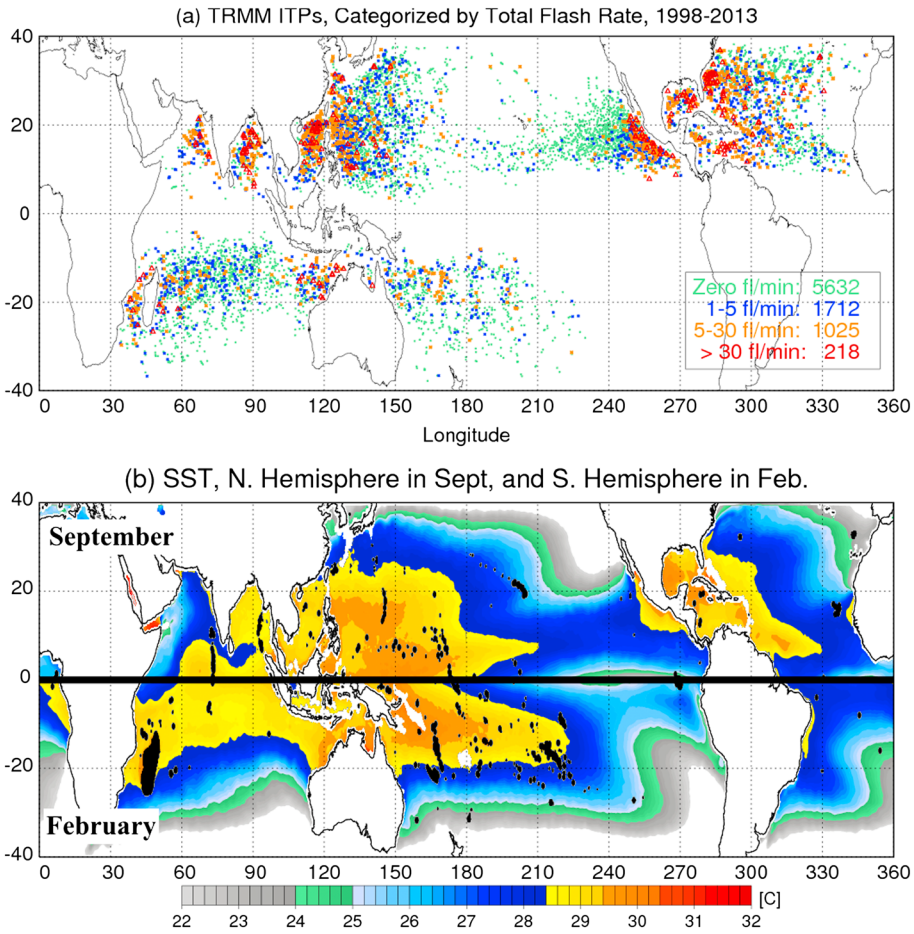

Figure 2. (a) Geographical distribution of TRMM ITPs over oceans > 100 km from the coast during 1998–2013. ITPs are categorized by total flash rate (fl min^{-1}) within 500 km radius from the TC center. (b) Monthly mean global SSTs, with Northern Hemisphere in September and Southern Hemisphere in February.

3.2. Radial Distribution

Figure 3 shows the mean FLD of TCs in various intensity categories as a function of radial distance from the TC center. Generally, FLD maximizes in both the INCO and OB regions (Figure 3a), and is a minimum in the region between the INCO and OB (100–200 km, Figure 3a). Similar lighting distributions (bimodal) were found in previous studies using various sources of measurements [*Molinari et al.*, 1999; *Cecil et al.*, 2002; *Abarca and Corbosiero*, 2011; *Jiang et al.*, 2013]. However, a monotonic lightning structure, that is, lightning density decreases monotonically outward from the TC center, was also reported [*Yokoyama and Takayabu*, 2008; *DeMaria et al.*, 2012; *Zhang et al.*, 2015]. The major factor responsible for this difference (monotonic versus bimodal structure) could be attributed to whether or not the actual precipitation area is considered for flash rate or FLD calculation. In this study, as well as *Cecil et al.* [2002] and *Jiang et al.* [2013], flash rate is normalized by satellite-based rain area as lightning is tightly coupled to precipitating clouds, whereas precipitation area was not considered in the flash rate/FLD calculation by *Yokoyama and Takayabu* [2008], *DeMaria et al.* [2012], and *Zhang et al.* [2015].

The lightning bimodal structure is the most evident for CAT35 storms, less for TS/TD systems, and least defined in CAT12 storms (Figure 3a). More detailed INCO structures (Figure 3b) show that FLD maximizes in the eyewall region (0–40 km) and decreases rapidly outside the eyewall. The region between the eyewall and OB (~50–150 km) is termed the inner rainband where convection is sporadic and of moderate intensity [*Cecil et al.*, 2002; *Jiang et al.*, 2013]. In short, eyewall FLD is about 3 times the FLD in the OB, while OB FLD is about 3 times that of the inner rainband FLD. The eyewall FLD in CAT35 TCs is about twice that of TD/TS and CAT12 TCs (Figure 3b), suggesting substantially stronger convective vigor and updrafts of eyewall convection

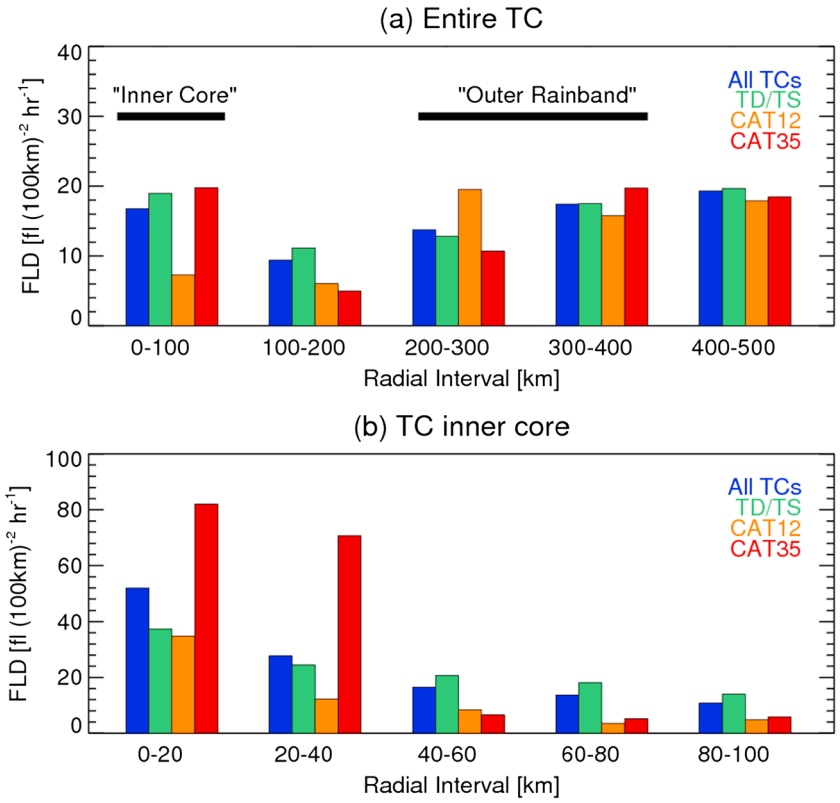

Figure 3. Mean lightning flash density as a function of radial distance from the TC center for TCs with various TC intensities: (a) lightning across the entire TC with 100 km interval and (b) lightning within the inner core region with 20 km interval. Note that TD/TS stand for tropical depression and tropical storm, CAT12 for category 1–2 TCs, and CAT35 for category 3–5 TCs.

in stronger TCs (CAT35 TCs). However, CAT35 TCs show a minimum of lightning activity in the inner rainband, resulting in a comparable FLD in the general INCO (0–100 km) as TD/TS storms (Figure 3a). Studies based on WWLLN data also find a similar (CG) lightning-sparse region between 50 and 150 km from the TC center [*DeMaria et al.*, 2012; *Stevenson et al.*, 2016]. Considering the variability of the eyewall extent, limited eyewall sampling, and consistency with previous studies, INCO (OB) is generally defined as the area within 0–100 (200–400) km radius of the TC center (Figure 3a).

3.3. Relationship to SST and Vertical Wind Shear

To better understand the variability of INCO and OB lightning, the FLD in these two regions have been examined as a function of SST and vertical wind shear (Figure 4). Generally, higher FLD in both the INCO and OB occur over warmer SSTs (Figure 4a), consistent with previous studies based on WWLLN [*Virts et al.*, 2015; *Stevenson et al.*, 2016]. Similarly, *Fierro and Mansell* [2017] showed that the introduction of cooler SST in TC simulations causes rapid decrease of lightning activity in both the INCO and OB. This is mainly because higher SSTs generate higher moisture and heat fluxes leading to higher moist static energy and greater instability [*Zhang and McPhaden,* 1995], promoting intense convection. Lightning activity is minimal over relatively cool SSTs (i.e., below 26°C), while FLD significantly increases for SST $>$ 27°C (for INCO) or 28°C (for OB). FLD for SSTs between 28 and 30°C is about 3–5 times greater compared to FLD for SST $<$ 26°C. Previous studies found that deep convection (for tropical convection in general) is mostly enhanced for SST $\geq$ 28°C as convective available potential energy (CAPE) is elevated under this condition, while CAPE is reduced and dominated by convective inhibition thus inhibits convection when SST $<$ 27°C [*Fu et al.*, 1994]. Therefore, the TC lightning-SST relationship discussed here is consistent with the relationship between general oceanic convection and SST found by *Fu et al.* [1994].

Significant differences also exist regarding the lightning-SST relationship between INCO (red bars) and OB (blue bars, Figure 4a). For SST $>$ 27°C, INCO FLD only increases slightly as SST increases, while the OB FLD

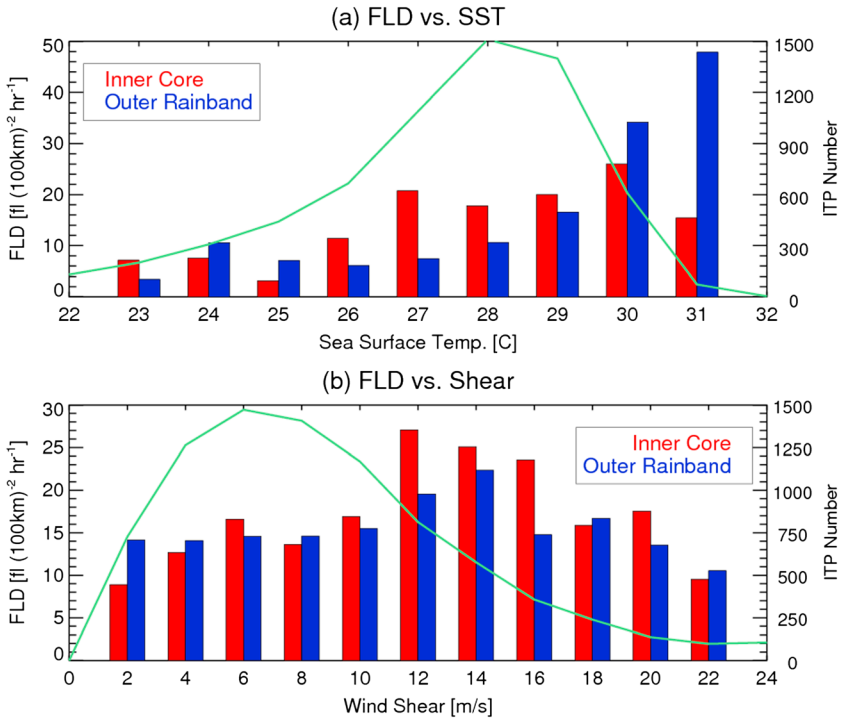

Figure 4. Total lightning flash density in the TC inner core and outer rainband regions as a function of (a) SST and (b) vertical wind shear (200–850 hPa). Sample of ITPs are shown by green curves.

increases remarkably with increasing SST. In other words, it appears that the INCO lightning activity is less sensitive to SST changes compared to OB lightning when SSTs reach a relatively high threshold ($>$ 27°C). Enhanced OB convection (lightning) under high SST conditions may act to suppress convection in the INCO [*Wang*, 2009], as deep convection in the OB can reduce the mass convergence into the eyewall [*Wang*, 2002], produce compensating subsidence over the eyewall [*Willoughby et al.*, 1984], and block or dilute the high potential temperature boundary layer inflow [*Wang*, 2002]. Also, INCO FLD maximizes at SST of 30°C and decreases at higher SST. In contrast, the OB FLD continues to increase for extreme SSTs. However, the significance of the FLD trends at SSTs $>$ 31°C is open to question given the limited sample size (~50 ITPs) involved.

Figure 4b shows TC lightning FLD as a function of environmental vertical wind shear (200–850 hPa). Both INCO and OB FLD peak at higher shear (12–16 m s^{-1}) environments, but INCO FLD shows a larger peak and greater shear-related variability. The INCO total lightning pattern in this study is generally consistent with studies based on WWLLN data [*Corbosiero and Molinari*, 2003; *DeMaria et al.*, 2012; *Zhang et al.*, 2015]. It is hypothesized that environments with stronger shear may enhance updrafts near the storm center by forcing TC asymmetries [*Corbosiero and Molinari*, 2003; *Fierro and Mansell*, 2017]. Environmental shear can tilt the vertical column of very high PV downshear in the INCO region and cause a secondary upward motion in the downshear region due to vortex balance [*Davis et al.*, 2008]. Environments with extreme shear may disrupt the TC's INCO structure and reduce the organization of eyewall convection leading to convective dissipation. On the other hand, the OB is outside of the high-PV region and OB convection (and lightning activity) is therefore less influenced by the shear-PV interaction [*DeMaria et al.*, 2012].

4. Relationship Between Total Lightning and TC Intensity Change

In order to guarantee valid 24 h TC intensity change, the ITPs are further restricted to be remaining over water and having valid intensity values within ±24 h of the TRMM overpass time. These restrictions reduce the sample from 8587 to 7432 ITPs for the investigation of TC intensity change. Figure 5 shows the distribution of ITPs as a function of +24 h intensity (MSW) change, which is defined as the MSW change during the 24 h period following each TRMM overpass (ITP). Of all ITPs, the 5th percentile and 95th percentile +24 h

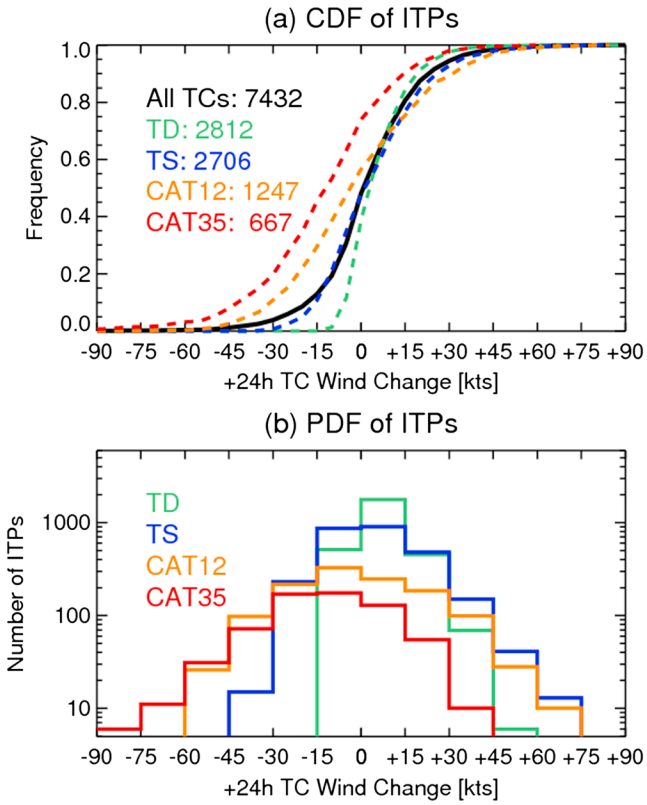

Figure 5. Distribution of ITPs as a function of TC intensity (maximum sustained wind speed) change in +24 h relative to the TRMM overpass: (a) cumulative distribution function and (b) probability distribution function. Labels in the *x* axis represent value bins as follows: −45 (−60 to −45), −30 (−45 to −30), −15 (−30 to −15), 0 (−15 to +15), +15 (+15 to +30), +30 (+30 to +45), etc.

intensity changes are around −30 kt and 30 kt (Figure 5a), given the 5 kt resolution of the best track data. Following previous studies, the 95th percentile (30 kt) and 5th percentile (−30 kt) of the 24 h intensity change will be used for defining RI and RW TCs. By this definition, our data set includes a large sample of TCs across various intensity changes (Figure 5b), e.g., 451 RI ITPs (compared to ~125 in *DeMaria et al.* [2012], 139 in *Tao and Jiang* [2015], and 170 in *Zhang et al.* [2015]). RI storms are mostly contributed by TCs of TS and CAT12 intensity, while RW mainly due to CAT12 and CAT35 TCs (Figure 5b). About 12% (8%) of the CAT12 (TD) storms experience RI, and 20% (10%) of the CAT35 (CAT12) hurricanes undergo RW (Figure 5a).

SST and vertical wind shear have been examined as a function of +24 h TC intensity change as shown in Figure 6. Generally, intensifying (weakening) TCs are associated with elevated (reduced) SSTs and reduced (increased) shear, consistent with previous TC intensity change studies [e.g., *Kaplan and DeMaria*, 2003]. However, SSTs and shear are not distinguishable between RI storms (>30 kt increase) and slowly intensifying TCs (increase of 15–30 kt). Similarly, *Hendricks et al.* [2010] found that environmental conditions (a set of variables including SST, shear, instability, and low-level humidity) are quite similar between RI TCs and slowly intensifying (non-RI) TCs in the NWPC and ATL basins. The false alarm ratio of forecasting RI remains undesirably high when only large-scale environmental parameters are included in the statistical TC intensity forecast model [*Kaplan and DeMaria*, 2010].

4.1. Relationships Between Lightning, Intense Convection, and TC Intensity Change

Figure 7 shows total lightning and our proxy for intense convection (VOL30) in the INCO and OB regions as a function of +24 h TC wind change. Of primary note is that both FLD and VOL30 are reduced in the INCO region of intensifying (>15 kt) TCs compared to neutral (−15 to 15 kt) and weakening (<15 kt) storms (Figures 7a and 7b). This finding, for total lightning (CG and IC), is consistent with CG lightning patterns observed by WWLLN [*DeMaria et al.*, 2012; *Stevenson et al.*, 2016], suggesting both types of lightning in the INCO region decrease for intensifying TCs. Furthermore, RI (>30 kt increase within 24 h) TCs produce substantially lower FLD in the INCO than slowly intensifying TCs (e.g., 15 kt increase), suggesting the potential use of total lightning information in forecasting RI. The consistency between LIS lightning measurements (FLD) and PR radar observations (VOL30) validates the lightning patterns in relationship to TC intensity change. VOL30 usually indicates the presence of large ice particles (e.g., hail/large graupel) owing to sufficient supercooled liquid water in the mixed phase region, necessary ingredients for electrification leading to lightning [*Petersen et al.*, 1999; *Liu et al.*, 2012]. To briefly summarize, intensifying TCs are associated with reduced INCO FLD/VOL30 with RI storms producing minimum FLD/VOL30 values, while neutral and weakening TCs show enhanced FLD/VOL30 in the INCO. These relationships between lightning and TC intensity change stay the

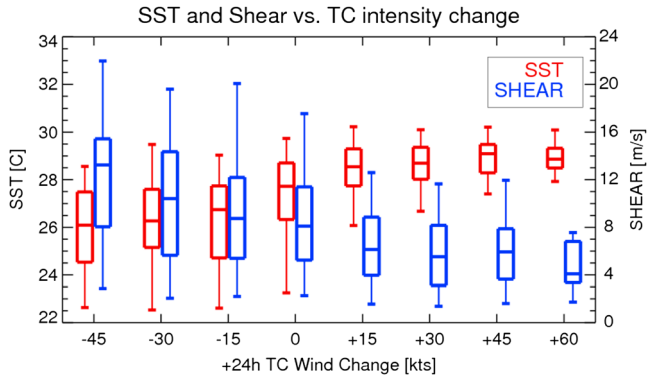

Figure 6. Distribution of SST and vertical wind shear during TRMM overpass as a function of TC intensity change in the +24 h. The box of the Whisker represents 25%, median, and 75% percentiles, while two ends of the Whisker stand for 2% and 98% percentiles, respectively. Labels in the *x* axis represent value bins as follows: −45 (−60 to −45), −30 (−45 to −30), −15 (−30 to −15), 0 (−15 to +15), +15 (+15 to +30), +30 (+30 to +45), etc. Only data bins with TRMM overpass sample number > 20 are shown.

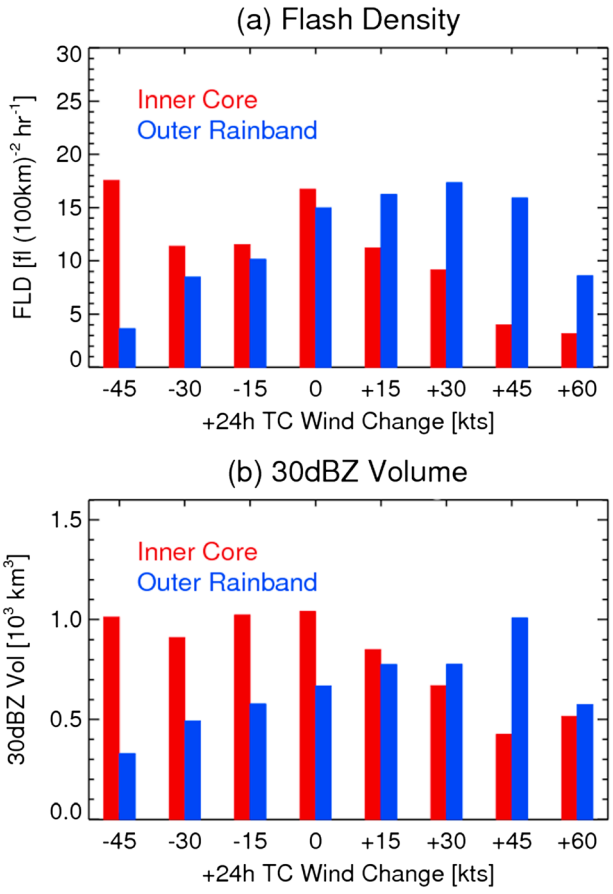

Figure 7. Lightning and radar convective proxy as a function of +24 h TC intensity change: (a) mean flash density (FLD) and (b) volume of radar reflectivity > 30 dBZ between −5 and −40°C (VOL30), which is normalized by the mean rain area. All red and blue bars represent inner core and outer rainband convection, respectively. Volume of 30 dBZ is normalized by ratio of rain area to the mean rain area of all ITPs.

same even when treating the CAT12 and CAT35 samples separately (e.g., with and without CAT35 ITPs in the data set, not shown). These negative relationships may be partially explained by the environmental shear differences between neutral/weakening TCs and intensifying TCs (Figure 6). As shown in Figure 4b, INCO FLD maximizes under strong shear conditions (12–16 m s^{-1}). However, 75% of the intensifying (or RI) TCs develop under low-to-moderate shear conditions (<8 m s^{-1}), which is not favorable for INCO lightning production (Figure 4b). In contrast, a significant portion (30%–50%) of neutral/weakening TCs occur in conditions of stronger shear (12–16 m s^{-1}), which promotes INCO lightning activity. As previously discussed, environments with stronger shear (compared to weakly sheared environments) may enhance updrafts near the storm center by forcing TC asymmetries [*Fierro and Mansell*, 2017]. The reason why FLD is reduced during RI but enhanced during TC weakening will be further discussed in section 5.2.

In contrast to INCO convection, FLD and VOL30 in the OB region show a generally positive relation with +24 h TC intensity change (blue bars in Figure 7). Intensifying TCs exhibit significantly greater FLD/VOL30 in the OB region than weakening TCs. OB FLD/VOL30 is, however, similar between slowly intensifying and RI TCs possibly owing to their similar SST and shear conditions (Figure 6). There is a slight trend for FLD/VOL30 to decrease in very rapidly intensifying TCs. As shown earlier, when SSTs exceed 27°C, OB lighting FLD increases significantly with further increase of SSTs (Figure 4a). However, INCO lightning activity changes only slightly as a function of SST (Figure 4a) when SST reaches above 27°C and is possibly more influenced by shear (Figure 4b). The OB is outside the high-PV region (INCO) thus less influenced by the interaction between environmental

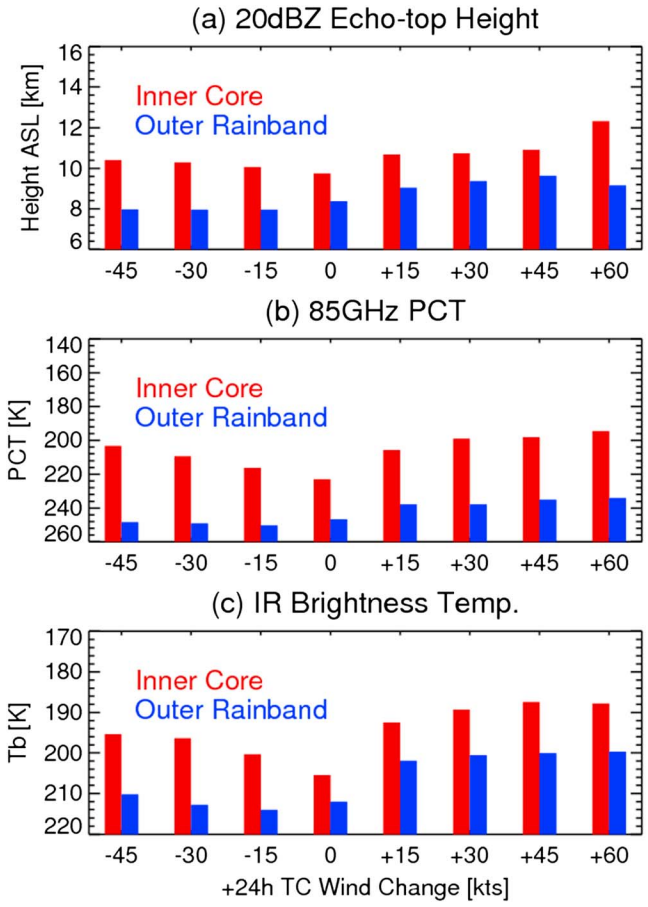

Figure 8. Same as Figure 7 but for TRMM convective proxies of (a) 20 dBZ echo top height (MAXHT20), (b) microwave polarization-corrected brightness temperature at 85 GHz (PCT85), and (c) infrared brightness temperature (IR Tb). Note that MAXHT20 are in 95% percentile, while PCT85 and IR Tb in the 5% percentile.

shear and PV [*Davis et al.*, 2008]. These observations may explain to some extent the opposite FLD/VOL30 patterns (in relation to TC intensity change) between the INCO and OB. In addition to the FLD trends, the comparison in FLD between INCO and OB is also interesting. INCO FLD is higher than OB FLD for weakening TCs, but this switches for intensifying or RI cases (Figure 7a), which is also reported regarding CG lightning patterns by *DeMaria et al.* [2012].

4.2. Relationships of MAXHT20, IR Tb, and PCT85 to TC Intensity Change

Figure 8 shows the convective depth (MAXHT20), microwave ice scattering signature (PCT85) and cold cloud top Tb (IR Tb) as a function of +24 h TC intensity change. Each of these convective-depth-related parameters in both the INCO and OB increases from neutral TCs to intensifying storms. For weakening TCs (24 h decrease $>$ 15 kt), greater convective depths and increased vertically integrated ice contents (indicated by PCT85) are present compared to neutral TCs, possibly because TC weakening mostly occurs in substantial TCs (CAT12 and CAT35, Figure 5). Convective depth and vertically integrated ice content are somewhat similar in RI and slowly intensifying TCs, consistent with previous studies [*Jiang and Ramirez*, 2013; *Tao and Jiang*, 2015]. In short, MAXHT20, IR Tb, and PCT85 in the INCO region show an opposite trend to FLD and VOL30 preceding TC intensification, especially RI. Lightning is correlated with the combination of vertically integrated ice content and the presence of supercooled cloud water [*Takahashi*, 1978; *Saunders et al.*, 2006]. In the INCO of intensifying TCs, overall convective depth and vertically integrated ice content are elevated but VOL30 and lightning activity are reduced, suggesting the possible lack of supercooled liquid content (required for formation of graupel) and establishment of glaciated conditions. Tall convective towers (e.g., hot towers) [*Kelley et al.*, 2004, 2005] in the INCO may lead to eyewall vorticity enhancement [*Montgomery et al.*, 2006] thus TC intensification. However, only a fraction of RI storms ($<$10%, not shown) have convective hot towers (i.e., MAXHT20 $>$ 14.5 km) in the INCO, suggesting that TRMM only observed a marginal relation between the presence of INCO hot towers and RI. In short, INCO deep convection appears to be linked to TC intensification, but our observations suggest that hot towers and abundant lightning-producing intense convection are not strong characteristics of TCs that undergo RI.

4.3. Lightning "Evolution" in Rapidly Intensifying and Weakening TCs

In order to test whether lightning shows any leading signal for TC intensity change, especially RI, this subsection examines the "evolution" (composite of TRMM overpasses in every 6 h) of lightning FLD for the RI TCs (Figure 9). Again, RI TCs are defined as 24 h MSW increase $>$ 30 kt. For comparison, evolution of weakening TCs are also included, which are defined as 24 h MSW decrease $>$ 15 kt. In the time line (x axis) of Figure 9, 0 h represents the onset of RI or weakening, while negative and positive values indicate before and after the

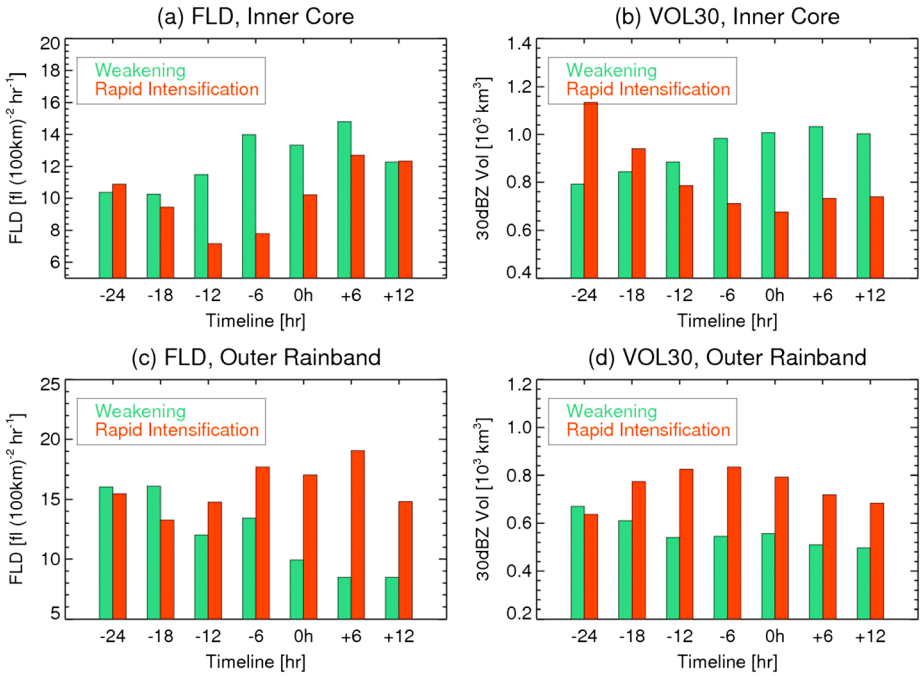

Figure 9. (a, c) Flash density and (b, d) 30 dBZ echo volume (VOL30) between −5 and −40°C in the inner core region (Figures 9a and 9b) and outer rainband region (Figures 9c and 9d), as a function of time period relative to the onset of TC weakening (green bars) and rapid intensification (red bars).

onset. This time evolution (Figure 9) is constructed in the following steps: (1) a TRMM overpass is identified, (2) search RI or weakening events within a 48 h time frame (−24 to +24) of the TRMM overpass, (3) derive the specific time of the TRMM overpass relative to the onset of the RI or weakening event (value in *x* axis of Figure 9), (4) composite all TRMM overpasses in each time interval through the RI/weakening lifecycle.

In the INCO region, FLD substantially decreases 12 h prior to the onset of RI and increases again during RI (red bars, Figure 9a). Similarly, *DeMaria et al.* [2012] found that eyewall lightning (CG) increase only occurs during or after RI. However, weakening TCs show an opposite INCO lightning evolution pattern: FLD starts to increase 6–12 h before TC weakening (green bars, Figure 9a). Weakening TCs produce significantly higher INCO FLD than RI TCs slightly prior to (−6 h) and during (0 h) intensity change, consistent with results in section 4.2. VOL30 in the INCO exhibits a similar evolution trend through the life cycle of RI and weakening TCs (Figure 9b). VOL30 decreases substantially leading up to RI, then remains steady during and after RI onset. This suggests that deep, vigorous convection, as marked by the volume containing mixed-phase microphysics (conducive to lightning production) decreases prior to the onset of RI. On the other hand, in weakening TCs, the opposite trend is observed.

Regarding the OB region, FLD begins increasing 6–12 h prior to RI onset and reaches a maximum 6 h after RI begins (Figure 9c). OB FLD decreases 12 h before TC starts weakening, and keeps decreasing during the TC weakening cycle. Similarly, VOL30 shows an increasing (decreasing) trend prior to RI (weakening) onset, although with a smaller magnitude (Figure 9d). Another interesting feature of RI TCs is that OB FLD (red bars in Figure 9c) is more than twice that of the INCO FLD (red bars in Figure 9a) 6–12 h preceding RI.

4.4. Does the Lightning-TC Intensity Change Relationship Depend on Prior TC Status?

Recent studies suggested that the relationship between eyewall convection and future TC intensity change (e.g., +24 h) may depend on preceding TC intensity change status. For example, the areas of INCO deep convection (20 dBZ radar echo top $>$ 12 km) is very similar between weakening, neutral, and RI TCs that spin-up from neutral status (so-called initial RI), whereas RI-continuing TCs (which have already underwent RI in the last 24 h) show substantially larger INCO deep convective areas [*Tao and Jiang*, 2015; *Alvey et al.*, 2015]. *Molinari et al.* [1999] proposed that weakening or slowly intensifying TCs are likely to intensify after a lightning burst in the INCO. To examine this hypothesis, our TC sample was broken down into three

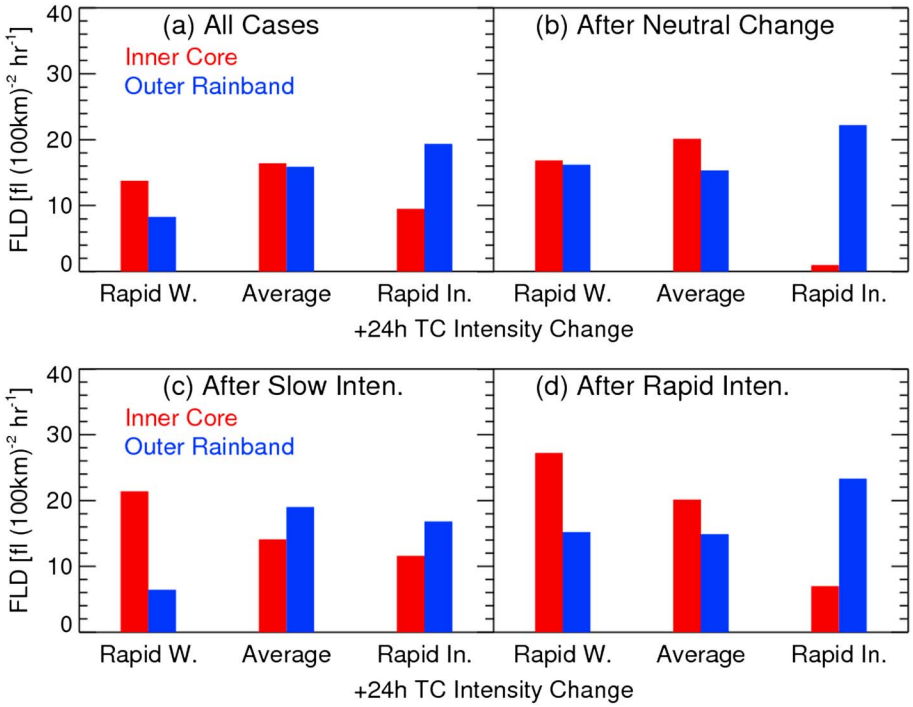

Figure 10. Flash density (FLD) in the INCO and OB regions as a function of +24 h TC intensity change: rapid weakening (+24 h wind change < -30 kt), average intensity change (-30 kt < -24 h wind change <30 kt), and rapid intensification (+24 h wind change > 30 kt). ITPs are categorized by (a) all cases, (b) TCs after neutral intensity change (-10 kt < -24 h wind change <10 kt), (c) TCs after slow intensification (10 kt < -24 h wind change <30 kt), and (d) TCs after rapid intensification (-24 h wind change > 30 kt).

categories based on the TC intensity change during the 24 h prior to TRMM overpass (-24 h): (1) neutral change, where MSW change is between -10 and 10 kts; (2) slow intensification (SI), where increase of MSW is between 10 and 30 kts; (3) RI, where increase of MSW exceeds 30 kts.

Figure 10 shows the mean values of FLD in the INCO and OB for RW (+24 h MSW decrease > 30 kt), average (+24 h MSW change between -30 and 30 kt), and RI (+24 h MSW increase > 30 kt) TCs. In general, RI TCs have the smallest INCO FLD but the greatest OB FLD, while RW TCs show similar INCO FLD but lower OB FLD compared to average TCs (Figure 4a). The "RI signal" (minimum INCO FLD but maximum OB FLD) is most evident for TCs that underwent little intensity change in the last 24 h (Figure 10b), but it is less defined for TCs after slow intensification (Figure 10c). It is interesting that the "RI signal" also applies to RI-continuing TCs (Figure 10d), suggesting that RI is more likely to continue if only minimum (maximum) INCO (OB) lightning occurs. RW TCs show enhanced INCO FLD but reduced OB FLD for TCs that already underwent intensification (especially RI) in the previous 24 h period (Figures 10c and 10d). This "RW signal" is not clear for TCs that experienced little change in the last 24 h (Figure 10b). Therefore, the onset of a lightning burst in the INCO may signal the end of TC intensification (or RI) and the onset of RW (consistent with *Molinari et al.* [1999] and *DeMaria et al.* [2012]).

5. Summary and Discussion

5.1. Summary

Previous studies suggested that lightning activity (mainly CG) could be an indicator of TC intensity change, but their relationships vary greatly and at times appear contradictory. This study leverages the 16 year total lightning data recorded by TRMM LIS to investigate (globally) the TC lightning characteristics and their relationships with TC intensity change, in parallel to analysis of TC convection observed by the TRMM PR, TMI, and VIRS. Results from this study can be summarized as follows:

1. Approximately 35% of the TRMM TC overpasses contain lightning, with TSs having the highest FLD and CAT35 TCs the lowest. TC total lightning shows a bimodal structure with FLD maximizing in both the

eyewall and OB regions and achieving a minimum in the inner rainband region between the eyewall and the OB.

2. Higher SST and strong vertical wind shear (12–16 m s^{-1}) promote maximum FLD in both the INCO and OB regions. However, when SST $>$ 27°C, INCO FLD only increases slightly as SSTs increase beyond this value, while OB FLD increases remarkably above this SST threshold, possibly due to the negative impact of OB convection on the INCO convection. INCO FLD shows greater variability than OB FLD in relation to shear, owing to the interaction between high potential vorticity (mainly in the INCO) and environmental shear.
3. INCO (OB) lightning is generally negatively (positively) correlated to TC intensity change in the next 24 h (+24 h), with intensifying TCs having lower FLD than weakening and neutral TCs. These lightning patterns are consistent to patterns of 30 dBZ echo volume in the mixed-phase region (VOL30), which is an indicator of convective intensity and the presence of robust mixed-phase microphysics. RI TCs (24 h wind increase $>$ 30 kt) also shows significantly smaller FLD and VOL30 than slowly intensifying TCs (24 h wind increase of 15–30 kt), indicating the potential of these parameters in forecasting RI.
4. In contrast to the INCO lightning and VOL30, TRMM parameters of convective depth and vertically integrated ice content (MAXHT20, PCT85, and IR Tb) in both the INCO and OB show an increasing trend from neutral to intensifying TCs, suggesting the lack of supercooled liquid content and establishment of glaciated conditions in the INCO of intensifying, especially RI TCs. Glaciated conditions are associated with reduced charge generation and lightning flash rates.
5. INCO FLD and VOL30 start to decrease 18 h preceding the onset of RI and reaches a minimum 6 h before RI, whereas they begin increasing 12 h prior to TC weakening. FLD and VOL30 in the OB region show opposite trends to FLD/VOL30 in the INCO.
6. The negative (positive) INCO (OB) lightning relationship with TC intensity change in the next 24 h (+24 h) generally persists regardless of prior (−24 h) TC intensity change status. However, the INCO signature of RI (i.e., suppressed INCO FLD) is the strongest for TCs that experienced little intensity change in the last 24 h, whereas the INCO signature of RW (i.e., enhanced INCO FLD) is the most evident for TCs that already underwent RI in the last 24 h.

5.2. Discussion

Since global lightning measurements became available from long-range lightning detection networks (e.g., WWLLN), many efforts have been directed toward determining the relationship between lightning and TC intensity change. However, findings from these CG-based studies have a large variance and in some cases appear contradictory (as reviewed at the beginning of this paper). By making use of the full spectrum of the large TRMM data set, this study improves the clarity of the relevant issues from multidimensional perspectives regarding TC convection, e.g., total lightning density, mixed-phase radar echo volume, echo top heights, and vertically integrated ice content. Using total lightning, we did not find that RI was preceded by an increase in eyewall lightning activity as some of the CG-based studies argued [*Lyons and Keen*, 1994; *Stevenson et al.*, 2014; *Susca-Lopata et al.*, 2015; *Zhang et al.*, 2015]. The studies that found eyewall lightning increases (or lightning bursts) prior to RI were however case study-based; thus, the generality of the finding is in question. For example, increases in eyewall CG lightning flashes were also found in individual weakening TCs [*Squires and Businger*, 2008; *Thomas et al.*, 2010]. Other studies found a strong positive correlation (r = 0.7–0.8) between CG lightning frequency and TC intensity for a significant number of major hurricanes [*Price et al.*, 2009; *Pan et al.*, 2014; *Whittaker et al.,* 2015]. These studies analyzed CG lightning flashes within the entire TC, not subdividing by the INCO and OB regions, the latter dominating the TC total area. These studies however are consistent with our findings for a positive relationship between total lightning in the OB and TC intensity change.

Findings from this study confirm the negative (positive) relationship between INCO (OB) CG lightning and TC intensity change found by *DeMaria et al.* [2012]. Both total lightning (this study) and CG lightning [*DeMaria et al.*, 2012] showed the following: (1) RI TCs have the least INCO lightning density, but the highest OB lightning density; (2) FLD in the INCO (or eyewall) increases 6–12 h preceding the onset of TC weakening, but decreases 12–18 h prior to TC intensification (or RI). However, there are also some specific differences and new details emerging from our study. For example, in RI TCs total lightning density is much lower in the INCO than in the OB (Figure 7a), while CG density in the INCO is higher than or close to OB CG density [Figure 8 in *DeMaria et al.*, 2012]. This may suggest a lower IC:CG ratio in the INCO of RI TCs. While

DeMaria et al. [2012] showed no changes of CG density in the OB preceding the onset of intensifying events (their Figure 6), this study demonstrates that total flash density in the OB increases significantly 6–12 h prior to the onset of RI (Figure 9c).

As mentioned above, one of the more intriguing findings in this study is that intensifying TCs (especially RI) are marked by significantly lower INCO lightning FLD and lower convective intensity (VOL30) than weakening or neutral TCs. Specifically, INCO FLD substantially decreases 12–18 h preceding the onset of RI but increases 6–12 h prior to TC weakening. However, OB lightning shows the opposite pattern in relation to TC intensity change. Similar differences between the INCO and OB FLD has also been reported for CG lightning density, and were proposed to be caused by the impact of PV tilting by vertical shear [*DeMaria et al.*, 2012]. Our results indicate that INCO lightning activity is more likely controlled by vertical wind shear of the TC environment (small variability with SST but significant variability with shear, as shown in Figure 4) provided favorable SST conditions (SST $>$ 27°C). Environmental shear can tilt the high PV column in the INCO leading to asymmetric but more vigorous convection [*Davis et al.*, 2008, *Corbosiero and Molinari*, 2003], which has been seen in many TCs [*Lyons and Keen*, 1994; *Molinari et al.*, 2006; *Squires and Businger*, 2008]. One example is that convection became very asymmetric and very intense (with large FLD) when Hurricane Gabrielle (2001) interacted with an upper level trough in the Gulf of Mexico [*Molinari et al.*, 2006]. Recent cloud-resolving model simulations also demonstrated that increased wind shear will induce a more asymmetric INCO and produce substantially higher INCO flash rates [*Fierro and Mansell*, 2017]. Enhanced asymmetric deep convection in the INCO may induce short-term intensification, but the negative effects of the vertical shear are detrimental to long-term intensification. On the other hand, the OB is less influenced by this shear-PV interaction but more influenced by convective instability of the storm environment (related to SST), as the OB is outside the high-PV region of the INCO [*DeMaria et al.*, 2012]. This is supported by the fact that OB lightning is sensitive to SST increase (Figure 4a) but only varies slightly as a function of shear (Figure 4b).

Another possible reason is that RI is more likely determined by the increase of symmetric convection instead of asymmetric intense convection (usually stronger than symmetric convection) in the INCO as proposed by recent studies [*Tao and Jiang*, 2015; *Alvey et al.*, 2015]. *Nolan and Grasso* [2003] and *Nolan et al.* [2007] showed that the intensification of the vortex near the storm center is mainly a symmetric response to the azimuthally averaged latent heating release and pure asymmetric heating has a very small impact on vortex intensification, suggesting the more important role of symmetric convection than asymmetric intense convection. *Jiang* [2012] reported that the 24 h RI probability remains the same between TCs with and without hot towers (e.g., 20 dBZ echo top height $>$ 14.5 km) in the inner-core region, suggesting that hot towers (or very intense convection) are neither a necessary nor a sufficient condition for RI. In contrast, recent studies showed that the best defined feature of RI TCs (distinguishable from non-RI TCs) is the higher degree of symmetry of the INCO convection, especially shallow-to-moderate convection [*Tao and Jiang*, 2015; *Alvey et al.*, 2015]. Compared to asymmetric TCs, symmetric TCs usually produce a limited amount of eyewall lightning due to their relatively weak updrafts [*Corbosiero and Molinari*, 2003; *Demetriades and Holle*, 2005]. Furthermore, supercooled liquid water, which is key for charge separation [*Takahashi*, 1978], may be lacking in symmetric eyewalls (or RI TCs). Ice particles generated in intense convective cells will be distributed more evenly throughout the eyewall (in the mixed-phase region), which could lead to depletion of the available supercooled liquid water through the riming process. In fact, this study shows that reduced INCO lightning and VOL30 (Figure 7) is accompanied by enhanced convective depth and vertically integrated ice content (Figure 8) in the INCO of RI TCs, which suggests the lack of supercooled liquid content and establishment of glaciated conditions in the eyewall of these TCs.

Acknowledgments
This research was supported by the NASA PMM grant NNX16AD85G (S. A. Rutledge, PI), NASA ROSES grant NNX17AH62G (W. Xu, PI), and the National Natural Science Foundation of China grant 41405004 (W. Zhang). We thank Mark DeMaria, the NHC Techology and Science branch chief, Daniel Cecil from University of Alabama-Huntsville, and the other anonymous reviewer for their constructive comments and suggestions. Our thanks also go to colleagues for insightful discussions of this work, especially John Knaff and Andrea Schumacher from CIRA. The TRMM satellite data can be downloaded from NASA Goddard Earth Sciences Data and Information Services Center (http://disc.sci.gsfc.nasa.gov/TRMM) and the TC best track data from NOAA NCDC (https://www.ncdc.noaa.gov/ibtracs/).

References

Abarca, S. F., and K. L. Corbosiero (2011), The World Wide Lightning Location Network and convective activity in tropical cyclones, *Mon. Weather Rev.*, *139*, 175–191.

Alvey, G. R., III, J. Zawislak, and E. Zipser (2015), Precipitation properties observed during tropical cyclone intensity change, *Mon. Weather Rev.*, *143*, 4476–4492.

Black, R. A., and J. Hallett (1999), Electrification of the hurricane, *J. Atmos. Sci.*, *56*, 2004–2028.

Boccippio, D. J., K. L. Cummins, H. J. Christian, and S. J. Goodman (2001), Combined satellite- and surface-based estimation of the intracloud–cloud-to-ground lightning ratio over the continental United States, *Mon. Weather Rev.*, *129*, 108–122.

Cecil, D. J., and E. J. Zipser (1999), Relationships between tropical cyclone intensity and satellite-based indicators of inner core convection: 85-GHz ice-scattering signature and lightning, *Mon. Weather Rev.*, *127*, 103–123.

Cecil, D. J., E. J. Zipser, and S. W. Nesbitt (2002), Reflectivity, ice scattering, and lightning characteristics of hurricane eyewalls and rainbands. Part I: Quantitative description, *Mon. Weather Rev.*, *130*, 769–784.
Cecil, D. J., D. E. Buechler, and R. J. Blakeslee (2015), TRMM LIS climatology of thunderstorm occurrence and conditional lightning flash rates, *J. Clim.*, *28*, 6536–6547.
Christian, H. J., et al. (2003), Global frequency and distribution of lightning as observed from space by the optical transient detector, *J. Geophys. Res.*, *108*(D1), 4005, doi:10.1029/2002JD002347.
Corbosiero, K. L., and J. Molinari (2003), The relationship between storm motion, vertical wind shear, and convective asymmetries in tropical cyclones, *J. Atmos. Sci.*, *60*, 366–376.
Davis, C. A., S. C. Jones, and M. Reimer (2008), Hurricane vortex dynamics during Atlantic extratropical transition, *J. Atmos. Sci.*, *65*, 714–736.
Dee, D. P., and S. Uppala (2009), Variational bias correction of satellite radiance data in the ERA-Interim reanalysis, *Q. J. R. Meteorol. Soc.*, *135*, 1830–1841, doi:10.1002/qj.493.
DeMaria, M., R. T. DeMaria, J. A. Knaff, and D. Molenar (2012), Tropical cyclone lightning and rapid intensity change, *Mon. Weather Rev.*, *140*, 1828–1842.
DeMaria, M., C. R. Sampson, J. A. Knaff, and K. D. Musgrave (2014), Is tropical cyclone intensity guidance improving?, *Bull. Am. Meteorol. Soc.*, *95*, 387–398.
Demetriades, N. W. S., and R. L. Holle (2005), Long-range lightning applications for hurricane intensity Preprints, Conf. on Meteorological Applications of Lightning Data, Am. Meteorol. Soc., pp. 2.8, San Diego, Calif. [Available at http://ams.confex.com/ams/pdfpapers/84498.pdf.]
Fierro, A. O., and J. M. Reisner (2011), High-resolution simulation of the electrification and lightning of Hurricane Rita during the period of rapid intensification, *J. Atmos. Sci.*, *68*, 477–494.
Fierro, A. O., X.-M. Shao, T. Hamlin, J. M. Reisner, and J. Harlin (2011), Evolution of eyewall convective events as indicated by intra- cloud and cloud-to-ground lightning activity during the rapid intensification of Hurricanes Rita and Katrina, *Mon. Weather Rev.*, *139*, 1492–1504.
Fierro, A. O., E. R. Mansell, C. L. Ziegler, and D. R. MacGorman (2015), Explicitly simulated electrification and lightning within a tropical cyclone based on the environment of Hurricane Isaac (2012), *J. Atmos. Sci.*, *72*, 4167–4193.
Fierro, A. O., and E. R. Mansell (2017), Electrification and lightning in idealized simulations of a hurricane-like vortex subject to wind shear and sea surface temperature cooling, *J. Atmos. Sci.*, *74*, 2023–2041.
Fu, R., A. D. Del Genio, and W. B. Rossow (1994), Influence of ocean surface conditions on atmospheric vertical thermodynamic structure and deep convection, *J. Clim.*, *7*, 1092–1108.
Gentemann, C. L., T. Meissner, and F. J. Wentz (2010), Accuracy of satellite sea surface temperatures at 7 and 11 GHz, *IEEE Trans. Geosci. Remote Sens.*, *48*, 1009–1018.
Goodman, S. J., et al. (2013), The GOES-R Geostationary Lightning Mapper (GLM), *Atmos. Res.*, *125–126*, 34–49.
Griffin, S. (2017), Climatology of tropical overshooting tops in North Atlantic tropical cyclones, *J. Appl. Meteorol. Climatol.*, doi:10.1175/JAMC-D-16-0413.1.
Guimond, S. R., G. M. Heymsfield, and F. J. Turk (2010), Multiscale observations of Hurricane Dennis (2005): The effects of hot towers on rapid intensification, *J. Atmos. Sci.*, *67*, 633–654.
Hence, D. A., and R. A. Houze Jr. (2011), Vertical structure of hurricane eyewalls as seen by the TRMM precipitation radar, *J. Atmos. Sci.*, *68*, 1637–1652.
Hendricks, E. A., M. T. Montgomery, and C. A. Davis (2004), The role of "vortical" hot towers in the formation of Tropical Cyclone Diana (1984), *J. Atmos. Sci.*, *61*, 1209–1232.
Hendricks, E. A., M. S. Peng, B. Fu, and T. Li (2010), Quantifying environmental control on tropical cyclone intensity change, *Mon. Weather Rev.*, *138*, 3243–3271.
Houze, R. A., Jr. (2010), Clouds in tropical cyclones, *Mon. Weather Rev.*, *138*, 293–344.
Jiang, H. (2012), The relationship between tropical cyclone intensity change and the strength of inner-core convection, *Mon. Weather Rev.*, *140*, 1164–1176.
Jiang, H., and E. M. Ramirez (2013), Necessary conditions for tropical cyclone rapid intensification as derived from 11 years of TRMM data, *J. Clim.*, *26*, 6459–6470.
Jiang, H., E. M. Ramirez, and D. J. Cecil (2013), Convective and rainfall properties of tropical cyclone inner cores and rainbands from 11 years of TRMM data, *Mon. Weather Rev.*, *141*, 431–450.
Kaplan, J., and M. DeMaria (2003), Large-scale characteristics of rapidly intensifying tropical cyclones in the North Atlantic basin, *Weather Forecasting*, *18*, 1093–1108.
Kaplan, J., and M. DeMaria (2010), A revised tropical cyclone rapid intensification index for the Atlantic and eastern North Pacific basins, *Weather Forecasting*, *25*, 220–241.
Kelley, O. A., J. Stout, and J. B. Halverson (2004), Tall precipitation cells in tropical cyclone eyewalls are associated with tropical cyclone intensification, *Geophys. Res. Lett.*, *31*, L24112, doi:10.1029/2004GL021616.
Kelley, O. A., J. Stout, and J. B. Halverson (2005), Hurricane intensification detected by continuously monitoring tall precipitation in the eyewall, *Geophys. Res. Lett.*, *32*, L20819, doi:10.1029/2005GL023583.
Khain, A. P., N. Cohen, B. Lynn, and A. Pokrovsky (2008), Possible aerosol effects on lightning activity and structure of hurricanes, *J. Atmos. Sci.*, *65*, 3652–3677.
Knaff, J. A., C. R. Sampson, M. DeMaria, T. P. Marchok, J. M. Gross, and C. J. McAdie (2007), Statistical tropical cyclone wind radii prediction using climatology and persistence, *Weather Forecasting*, *22*, 781–791.
Knapp, K. R., M. C. Kruk, D. H. Levinson, H. J. Diamond, and C. J. Neumann (2010), The International Best Track Archive for Climate Stewardship (IBTrACS): Unifying tropical cyclone best track data, *Bull. Am. Meteorol. Soc.*, *91*, 363–376.
Kummerow, C., W. Barnes, T. Kozu, J. Shiue, and J. Simpson (1998), The Tropical Rainfall Measuring Mission (TRMM) sensor package, *J. Atmos. Oceanic Technol.*, *15*, 808–816.
Kossin, J. P., and M. Sitkowski (2009), An objective model for identifying secondary eyewall formation in hurricanes, *Mon. Weather Rev.*, *137*, 876–892.
Lang, T. J., S. A. Rutledge, J. E. Dye, M. Venticinque, P. Laroche, and E. Defer (2000), Anomalously low negative cloud-to-ground lightning flash rates in intense convective storms observed during STERAO-A, *Mon. Weather Rev.*, *128*, 160–173.
Lang, T. J., and S. A. Rutledge (2002), Relationship between convective storm kinematics, precipitation, and lightning, *Mon. Weather Rev.*, *130*, 2492–2506.
Liu, C., D. J. Cecil, E. J. Zipser, K. Fronfeld, and R. Robertson (2012), Relationships between lightning flash rates and radar reflectivity vertical structures in thunderstorms over the tropics and subptropics, *J. Geophys. Res.*, *117*, D06212, doi:10.1029/2011JD017123.

Lyons, W. A., and C. S. Keen (1994), Observations of lightning in convective supercells within tropical storms and hurricanes, *Mon. Weather Rev.*, *122*, 1897–1916.
McCaul, E. W., D. E. Buechler, S. Hodanish, and S. J. Goodman (2002), The Almena, Kansas, tornadic storm of 3 June 1999: A long-lived supercell with very little cloud-to-ground lightning, *Mon. Weather Rev.*, *130*, 407–415.
Molinari, J., P. Moore, and V. Idone (1999), Convective structure of hurricanes as revealed by lightning locations, *Mon. Weather Rev.*, *127*, 520–534.
Molinari, J., P. Dodge, D. Vollaro, K. L. Corbosiero, and F. D. Marks Jr. (2006), Mesoscale aspects of the downshear reformation of a tropical cyclone, *J. Atmos. Sci.*, *63*, 341–354.
Montgomery, M. T., M. E. Nicholls, T. A. Cram, and A. B. Saunders (2006), A vortical hot tower route to tropical cyclogenesis, *J. Atmos. Sci.*, *63*, 355–386.
Montgomery, M. T., and R. K. Smith (2011), Paradigms for tropical-cyclone intensification, *Q. J. R. Meteorol. Soc.*, *137*, 1–31.
Nolan, D. S., and L. D. Grasso (2003), Nonhydrostatic, three-dimensional perturbations to balanced, hurricane-like vortices. Part II: Symmetric response and nonlinear simulations, *J. Atmos. Sci.*, *60*, 2717–2745.
Nolan, D. S., Y. Moon, and D. P. Stern (2007), Tropical cyclone intensification from asymmetric convection: Energetics and efficiency, *J. Atmos. Sci.*, *64*, 3377–3405.
Pan, L., X. Qie, and D. Wang (2014), Lightning activity and its relation to the intensity of typhoons over the Northwest Pacific Ocean, *Adv. Atmos. Sci.*, *31*, 581–592.
Petersen, W. A., R. C. Cifelli, S. A. Rutledge, B. S. Ferrier, and B. F. Smull (1999), Shipborne dual-Doppler operations during TOGA COARE: Integrated observations of storm kinematics and electrification, *Bull. Am. Meteorol. Soc.*, *80*, 81–97.
Price, C., M. Asfur, and Y. Yair (2009), Maximum hurricane intensity preceded by increase in lightning frequency, *Nat. Geosci.*, *2*, 329–332.
Reap, R. M., and D. R. MacGorman (1989), Cloud-to-ground lightning: Climatological characteristics and relationships to model fields, radar observations, and severe local storms, *Mon. Weather Rev.*, *117*, 518–535.
Rogers, R. (2010), Convective-scale structure and evolution during a high-resolution simulation of tropical cyclone rapid intensification, *J. Atmos. Sci.*, *67*, 44–70.
Rogers, R., P. Reasor, and S. Lorsolo (2013), Airborne Doppler observations of the inner-core structural differences between intensifying and neutral tropical cyclones, *Mon. Weather Rev.*, *141*, 2970–2991.
Saunders, C. P. R., H. Bax-Norman, C. Emersic, E. E. Avila, and N. E. Castellano (2006), Laboratory studies of the effect of cloud conditions on graupel/crystal charge transfer in thunderstorm electrification, *Q. J. R. Meteorol. Soc.*, *132*, 2653–2673.
Squires, K., and S. Businger (2008), The morphology of eyewall lightning outbreaks in two category 5 hurricanes, *Mon. Weather Rev.*, *136*, 1706–1726.
Steranka, J., E. B. Rodgers, and R. C. Gentry (1986), The relationship between satellite measured convective bursts and tropical cyclone intensification, *Mon. Weather Rev.*, *114*, 1539–1546.
Stevenson, S. N., K. L. Corbosiero, and J. Molinari (2014), The convective evolution and rapid intensification of Hurricane Earl (2010), *Mon. Weather Rev.*, *142*, 4364–4380.
Stevenson, S. N., K. L. Corbosiero, and S. F. Abarca (2016), Lightning in eastern North Pacific tropical cyclones: A comparison to the North Atlantic, *Mon. Weather Rev.*, *144*, 225–239.
Susca-Lopata, G., J. Zawislak, E. J. Zipser, and R. F. Rogers (2015), The role of observed environmental conditions and precipitation evolution in the rapid intensification of Hurricane Earl (2010), *Mon. Weather Rev.*, *143*, 2207–2223.
Takahashi, T. (1978), Riming electrification as a charge generation mechanism in Thunderstorms, *J. Atmos. Sci.*, *35*, 1536–1548.
Tao, C., and H. Jiang (2015), Distributions of shallow to very deep precipitation/convection in rapidly intensifying tropical cyclones, *J. Clim.*, *28*, 8791–8824.
Thomas, J. N., N. N. Solorzano, S. A. Cummer, and R. H. Holzworth (2010), Polarity and energetics of inner core lightning in three intense North Atlantic hurricanes, *J. Geophys. Res.*, *115*, A00E15, doi:10.1029/2009JA014777.
Toracinta, E. R., D. J. Cecil, E. J. Zipser, and S. W. Nesbitt (2002), Radar, passive microwave, and lightning characteristics of precipitating systems in the tropics, *Mon. Weather Rev.*, *130*, 802–824.
Vigh, J. L., and W. H. Schubert (2009), Rapid development of the tropical cyclone warm core, *J. Atmos. Sci.*, *66*, 3335–3350.
Virts, K. S., J. M. Wallace, M. L. Hutchins, and R. H. Holzworth (2015), Diurnal and seasonal lightning variability over the Gulf Stream and Gulf of Mexico, *J. Atmos. Sci.*, *72*, 2657–2665.
Wang, Y. (2002), Vortex Rossby waves in a numerically simulated tropical cyclone. Part II: The role in tropical cyclone structure and intensity changes, *J. Atmos. Sci.*, *59*, 1239–1262.
Wang, Y. (2009), How do outer spiral rainbands affect tropical cyclone structure and intensity?, *J. Atmos. Sci.*, *66*, 1250–1273.
Whittaker, I. C., E. Douma, C. J. Rodger, and T. J. C. H. Marshall (2015), A quantitative examination of lightning as a predictor of peak winds in tropical cyclones, *J. Geophys. Res. Atmos.*, *120*, 3789–3801, doi:10.1002/2014JD022868.
Willoughby, H. E., H.-L. Jin, S. J. Lord, and J. M. Piotrowicz (1984), Hurricane structure and evolution as simulated by an axisymmetric, non-hydrostatic numerical model, *J. Atmos. Sci.*, *41*, 1169–1186.
Xu, W., E. J. Zipser, C. Liu, and H. Jiang (2010), On the relationship between lightning frequency and thundercloud parameters of regional precipitation systems, *J. Geophys. Res.*, *115*, D12203, doi:10.1029/2009JD013385.
Yokoyama, C., and Y. N. Takayabu (2008), A statistical study on rain characteristics of tropical cyclones using TRMM satellite data, *Mon. Weather Rev.*, *136*, 3848–3862.
Zhang, G. J., and M. J. McPhaden (1995), The relationship between sea surface temperature and latent heat flux in the equatorial Pacific, *J. Clim.*, *8*, 589–605.
Zhang, W., Y. Zhang, D. Zheng, F. Wang, and L. Xu (2015), Relationship between lightning activity and tropical cyclone intensity over the northwest Pacific, *J. Geophys. Res. Atmos.*, *120*, 4072–4089, doi:10.1002/2014JD022334.